Soil Dynamics and Earthquake Engineering 177 (2024) 108408

Contents lists available at ScienceDirect

Soil Dynamics and Earthquake Engineering

journal homepage: www.elsevier.com/locate/soildyn

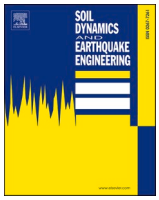

Equivalent fundamental period of bridge piers on caisson foundations from dynamic centrifuge testing

Domenico Gaudio [a,*,1], Gopal S.P. Madabhushi [a], Sebastiano Rampello [b], Giulia M.B. Viggiani [a]

[a] Department of Engineering, University of Cambridge, Cambridge, UK
[b] Dipartimento di Ingegneria Strutturale e Geotecnica, Sapienza Università di Roma, Rome, Italy

ARTICLE INFO

Keywords:
Caisson foundations
Bridge piers
Dynamic centrifuge test
Fundamental period
Inertial interaction

ABSTRACT

Dynamic soil-structure interaction is typically decomposed in kinematic and inertial effects. Inertial interaction generally results in an increase in the fundamental period and damping of the system, which, for slender structures, corresponds to a decrease of the inertial forces transmitted to the superstructure. Relations to estimate the period increase are mainly available in the literature for shallow foundations.

In this paper, the fundamental period of bridge piers on compliant caisson foundations was obtained from dynamic centrifuge tests. A rigid and a flexible bridge pier were subjected to trains of sinusoidal waves and real ground motions. The interpretation of the experimental results permitted to (i) evaluate the increase of period with respect to fixed-base conditions; (ii) assess the dependency of the compliant-base period on the motion intensity. The second aspect sheds light on the role played by non-linearity of soil behaviour and emphasises the importance of performing preliminary soil response analyses.

1. Introduction

Embedded, rigid and massive caisson foundations are typically adopted for bridge piers when high-intensity horizontal forces are to be resisted, *e.g.*, in the presence of marginally stable slopes or in highly seismic areas [1–3]. Their seismic behaviour has been attracting increasing interest by researchers in recent years, mainly due to the complex interaction phenomena with the soil and the superstructure, usually referred to as kinematic and inertial interaction effects.

Several authors have studied the seismic response of caisson foundations supporting bridge piers, either adopting the substructure method [4,5] or by advanced nonlinear dynamic analyses [6–8]. Very few works have tackled the problem by experimental investigation. Following the concept put forward by Gazetas [9] and Pecker [10] and based on the results of dynamic centrifuge tests, Gaudio et al. [11] suggested adopting the new Reversed Capacity Design method for these geotechnical systems. In turn, this design approach also stimulated research on the ultimate conditions of caisson foundations, in terms of their failure envelopes (*i.e.*, interaction diagrams) [12,13].

The fundamental compliant-base period T_{eq} plays a key role in the seismic response of superstructures with embedded foundations [14,15], as it can be adopted to compute the period lengthening due to dynamic soil-structure interaction effects and therefore determine whether interaction effects are to be accounted for or if, conversely, the fixed-base assumption may be considered adequate [16]. At a preliminary design stage, this period can be estimated by resorting to simplified Lumped-Parameter Models (LPM), where the superstructure is modelled with a Single Degree of Freedom (SDoF) oscillator and the soil-caisson system is replaced by dynamic impedance functions representing the additional contribution of the foundation soil to the compliance and damping of the entire soil-caisson-pier-deck system [1,17–20].

At an even lower level of complexity, the compliant-base period can also be computed from analytical [21–24] or empirical [25] relationships already available in the literature. When adopted for piers of long-span bridges, these equations typically result in a shift from the *plateau* to the descending tail of the design spectra prescribed by the national codes, rather than along the initial ascending portion of the spectra, as would be the case for squat structures. This corresponds to a significant reduction of the inertial forces transmitted to the bridge pier, relative to those obtained using the fixed-base period, T_s, provided that high-period ground motions, such as *e.g.*, those recorded in the Mexico

* Corresponding author. Dipartimento di Ingegneria Strutturale e Geotecnica Via Eudossiana 18, 00184, Rome, Italy.
E-mail address: domenico.gaudio@uniroma1.it (D. Gaudio).
[1] present address: Dipartimento di Ingegneria Strutturale e Geotecnica, Sapienza Università di Roma, Rome, Italy.

https://doi.org/10.1016/j.soildyn.2023.108408
Received 12 July 2023; Received in revised form 5 December 2023; Accepted 10 December 2023

City earthquake of 1985 [26] are not anticipated for the site under consideration. The reliability of these relationships, however, should be validated experimentally as most of them derive from the extrapolation of results obtained for shallow foundations, with embedment ratios $H/D \leq 1.5$.

In this paper, the equivalent compliant-base period T_{eq} of caisson foundations supporting bridge piers was determined experimentally from the results of dynamic centrifuge tests on reduced-scale models. These included a rigid and a flexible bridge pier founded on a cylindrical caisson embedded in a soft clay deposit overlain by a layer of sand. The two systems were subjected to a series of single-frequency sinusoidal and real ground motions. The analysis of the experimental results obtained from the reduced-scale models allowed estimating the fundamental period of the system, T_{eq}, and evaluating its increase with respect to the fixed-base period, T_s, and its dependency on input motion intensity. The latter aspect permitted to identify the key role of nonlinear soil behaviour on the fundamental period, T_{eq}. A comparison with the values computed adopting literature relationships is provided, which shows how to consider the dependency of T_{eq} on the ground motion intensity and provides an experimental validation of the relationships available in the literature. The two points made in this study may have useful implications in the design of critical infrastructures where caisson foundations are typically adopted, such as long-span bridges.

2. Problem definition

Fig. 1 shows the problem under examination, *i.e.*, the transverse response of a bridge pier founded on a cylindrical, concrete (unit weight $\gamma_c = 25.0$ kN/m^3) caisson subjected to a seismic input along the horizontal direction (x). A long span scheme is considered ($L_s > 40$ m), which ensures that both the influence of adjacent piers and the stiffness of the deck can be neglected. Here it is worth mentioning that the relative influence of two adjacent piers can be neglected even with values of the span length lower than 40 m, provided that the caisson distance is sufficient to exclude interaction phenomena between the two foundations. The caisson is characterised by a diameter $D = 8$ m and a height $H = 8$ m (slenderness ratio $H/D = 1$) for a total mass $m_c = 1024.8$ Mg, and is embedded in a deposit consisting of a loose sand layer of thickness $h_1 = 3$ m underlain by a soft clay stratum with thickness $h_2 = 14$ m. The water table is located at the sand-clay interface ($z_w = 3$ m) and the pore pressure regime is hydrostatic.

Typical piers for highway bridges with continuous pre-stressed concrete decks have diameters ranging between 1.0 and 2.5 m, depending on factors such as pier height and structural arrangement. In this study, two piers with the same height $h_s = 15$ m and different diameters, namely $d_p = 2.2$ and $d_p = 1.6$ m, were considered, with deck masses $m_d = 194.4$ and $m_d = 280.8$ Mg, representing span lengths $L_s = 50.0$ and 70.0 m respectively, the latter value representing an upper-bound for continuous pre-stressed concrete decks. These dimensions were selected with the twofold objective of being representative of highway bridges and of providing different fixed-base periods for the bridge piers (one twice the other), for almost the same total weight of the structure. The fixed base, fundamental period of the rigid and flexible pier, $T_s = 0.57$ and $T_s = 1.19$ s, respectively, was obtained considering the analytical solution for a cantilever beam with distributed and tip mass. The complete list of both geometric and mechanical parameters defining the problem is given in Table 1, where m_p is the pier mass and k_s is its flexural stiffness.

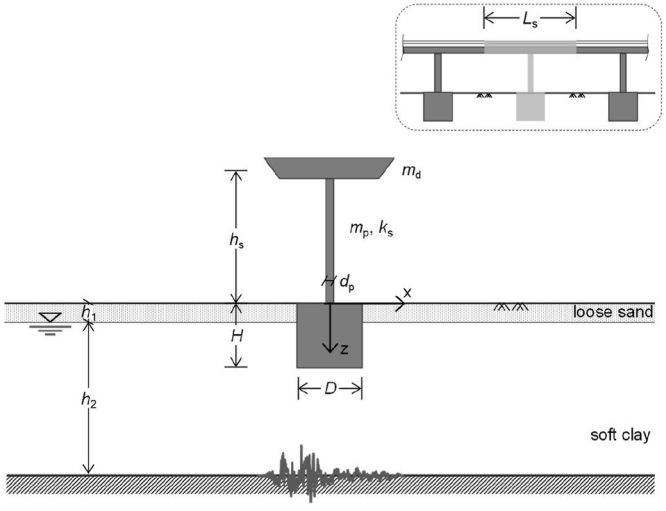

Fig. 1. Schematic layout of the problem.

3. Geotechnical centrifuge modelling

The seismic behaviour of the prototype bridge piers on caisson foundations described above was studied experimentally, by centrifuge testing of reduced-scale models. The models were subjected to an increased gravity of 60g, and geometrically scaled using a factor $N = 60$. Table 2 summarises the relevant scaling laws [27].

Fig. 2 shows pictures of the rigid and flexible systems as modelled in the centrifuge. The bridge piers were reproduced using a solid aluminium rod (alloy 6082-T6, unit weight $\gamma_{al} = 27.0$ kN/m^3) whose dimensions d_r and h_r are given in Table 3, while the deck mass was simulated though a brass cylinder (alloy CZ121, $\gamma_{br} = 85.6$ kN/m^3) with diameter d_d and height h_d. The resulting masses and fixed-base period at model scale are also given in Table 3. Here it is worth mentioning that the fixed-base periods of the models were slightly different from those estimated in the previous section, due to unavoidable differences between the desired prototype and model dimensions made in the laboratory. The fixed-base periods were obtained experimentally from the free-oscillations of the piers clamped at the base and subjected to a horizontal pulse at the top mass with a hammer, which provided periods $T_s = 0.0083{*}N \sim 0.50$ s and $T_s = 0.0156{*}N \sim 0.94$ s for the rigid and flexible system, respectively. These periods are those that will be taken as a reference in the following. 6082-T6 aluminium alloy was used to make the caissons adopted in both tests DG01 (rigid pier) and DG02 (flexible pier), consisting of a hollow cylinder ($d_{hole} = 46.10$ mm) closed at both ends by two aluminium plates, whose dimensions are given in Table 4. This hollow configuration was adopted to compensate the difference in the unit weight of aluminium and reinforced concrete. The same Hostun sand (HN31) used to create the shallow sand layer was glued to the surface of the caisson to mimic a rough soil-concrete contact. The white area visible along the shaft in Fig. 2b for the flexible system is due to the foundation having already been used in the previous test. Table 5 lists the physical and mechanical properties of Hostun sand, where G_s is the specific gravity, e_{max} and e_{min} are the maximum and minimum void ratio, and φ'_{cv} is the friction angle at critical state.

To reduce dynamic boundary effects [29], the reduced scale models were created into an Equivalent Shear Beam (ESB) container [30]. Fig. 3 shows a cross section of the model with the layout of the instrumentation adopted in the tests. Hostun sand was poured on the clay layer through a funnel and then finally levelled to obtain the desired thickness (50 mm at model scale). The clay was obtained by mixing speswhite kaolin powder with de-aired water (1:1.30 ratio by weight) to get a slurry, which was then one dimensionally consolidated through combined mechanical loading at the top and applied suction at the bottom of the clay layer. As discussed in the following, this consolidation procedure, previously reported by Garala and Madabhushi [31], permitted to obtain a soft clay layer providing a static safety factor $F_{SV} = N_{lim}/[(m_d + m_p)\cdot g]$ against bearing capacity high enough for the caissons to be the "lightly-loaded" ($F_{SV} \geq 5$ [6]), so as not to trigger irreversible soil response. To this end, the clay sample was consolidated under a vertical stress applied at the top of the clay layer equal to 512 kPa for test DG01

Table 1
Geometric and mechanical properties of the systems at prototype scale.

system	d_p (m)	h_s (m)	L_s (m)	m_p (Mg)	m_d (Mg)	k_s (MN/m)	T_s (s)	D (m)	H (m)	m_c (Mg)
rigid	2.20	15.0	50.0	143.6	194.4	27.3	0.57	8.0	8.0	1024.8
flexible	1.60	15.0	70.0	76.5	280.8	7.7	1.19	8.0	8.0	1024.8

Table 2
Scaling laws for dynamic centrifuge modelling (model/prototype).

length	mass	force	bending moment	flex. stiffness	time	frequency	acceleration	velocity	displacement
$1/N$	$1/N^3$	$1/N^2$	$1/N^3$	$1/N$	$1/N$	N	N	1	$1/N$

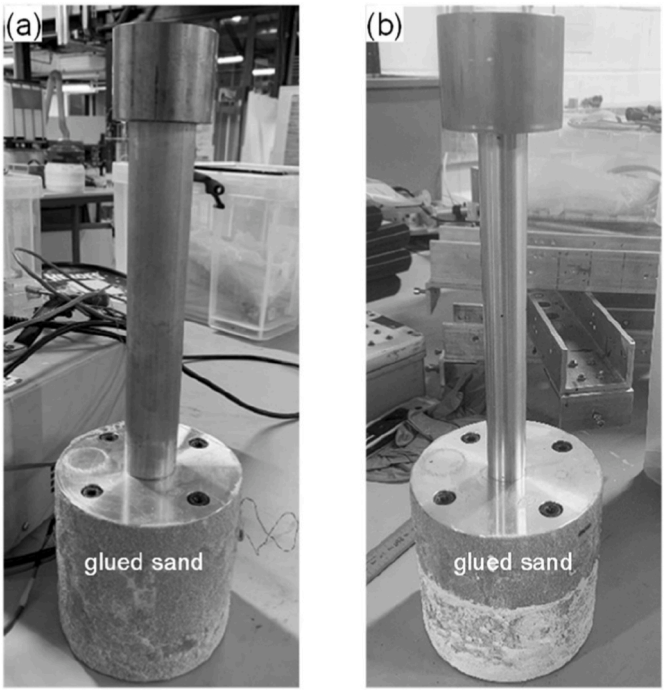

Fig. 2. Caisson-bridge system considered in: (a) DG01 and (b) DG02 tests.

and 256 kPa for test DG02, while the same suction of - 90 kPa was applied in both cases. This permitted to obtain an undrained shear strength, s_u, of about 44 and 26 kPa at depth $z = H + D/4$, as discussed in the following section, yielding a safety factor $F_{SV} = 10.2$ and 5.8 for tests DG01 and DG02, respectively. The vertical capacity of the caissons was computed using the equation provided by Gerolymos *et al.* [12], adapted for cylindrical caissons: $N_{lim} = 9.64\, A{\cdot}s_u{\cdot}(1 + H/D)^{0.67}$, where $A \approx 50.3$ m^2 is the cross-sectional area of the caisson. Table 6 summarises the properties of the speswhite kaolin used to create the clay layer, where w_L, w_P and *PI* are the liquid limit, plastic limit and plasticity index; λ and κ are the slopes of the Normal Compression Line and of the unloading-reloading lines in the *v*-*p*' plane; Γ and *M* are the intercept of the Critical State Line in the *v*-*p*' plane at $p' = 1$ kPa and the slope the CSL in the *q*-*p*' plane.

After unloading and removing the clay sample from the 1D consolidometer, its surface was trimmed to obtain the desired depth of 233 mm. The structure was then installed into a pre-drilled hole, with a diameter larger than the that of the caisson by about 2 mm, to minimise disturbance of the clay. After installing the superstructure, the gap between the model caisson and the clay was filled with speswhite kaolin slurry. The initial verticality of the structure was checked with a bubble level. This procedure reproduces the reduction of horizontal effective stress induced by caisson construction during the excavation stages (conventional under-excavation or shaft sinking), before installation of the steel reinforcement and concrete casting [33].

The instrumentation adopted in the two tests was the same. It included both instruments installed in the soil, such as the far-field alignments of Pore Pressure Transducers (PPTs, P_1–P_4) and piezoelectric accelerometers (A_1-A_6), and one PPT, P_5, and one piezoelectric accelerometer, A_7, located beneath the caisson and instruments mounted onto the structure, such as the Micro-Electro-Mechanical Systems (MEMS) glued on the brass mass at the top of the pier ($M_{1\text{-}4}$) and on the caisson ($M_{5\text{-}8}$), and two Linear Variable Differential Transformers (LVDT) ($L_{2\text{-}3}$) to measure the average settlement and rigid rotation of the caisson. LVDT L_1 was placed on the soil surface along the far-field alignment on the left of the model to record the far-field settlement accumulating during the test and relative to which the settlement of the structure should be computed.

3.1. Far-field soil mechanical properties

An Air Hammer Device (AHD) [34] at the base of the sand layer and a T-bar penetrometer [35], were used in flight to obtain the far-field profiles of small-strain shear modulus, G_0 (*z*), and of initial undrained shear strength of the soft clay stratum, s_u (*z*), respectively. The small-strain shear modulus at discrete depths z_i was calculated from the

Table 4
Geometric and mechanical properties of the caisson foundation at model scale (same for DG01 and DG02).

item	D (mm)	H (mm)	d_{hole} (mm)	m (kg)
hollow cylinder (1)	133.33	82.53	46.10	2.793
plate (2)	133.33	25.40	/	0.974
caisson = (1) + (2)x2	133.33	133.33	/	4.700

Table 5
Physical properties of the Hostun sand adopted in the dynamic centrifuge tests [28].

G_s (−)	e_{max} (−)	e_{min} (−)	φ'_{cv} (°)
2.65	1.010	0.555	33

Table 3
Geometric and mechanical properties of the superstructures at model scale.

system	test	d_r (mm)	h_r (mm)	d_d (m)	h_d (m)	$m_r = m_p$ (kg)	m_d (kg)	T_s (s)
rigid	DG01	37.3	228.0	55.6	44.5	0.665	0.900	0.0083
flexible	DG02	26.2	224.5	61.4	50.0	0.354	1.300	0.0156

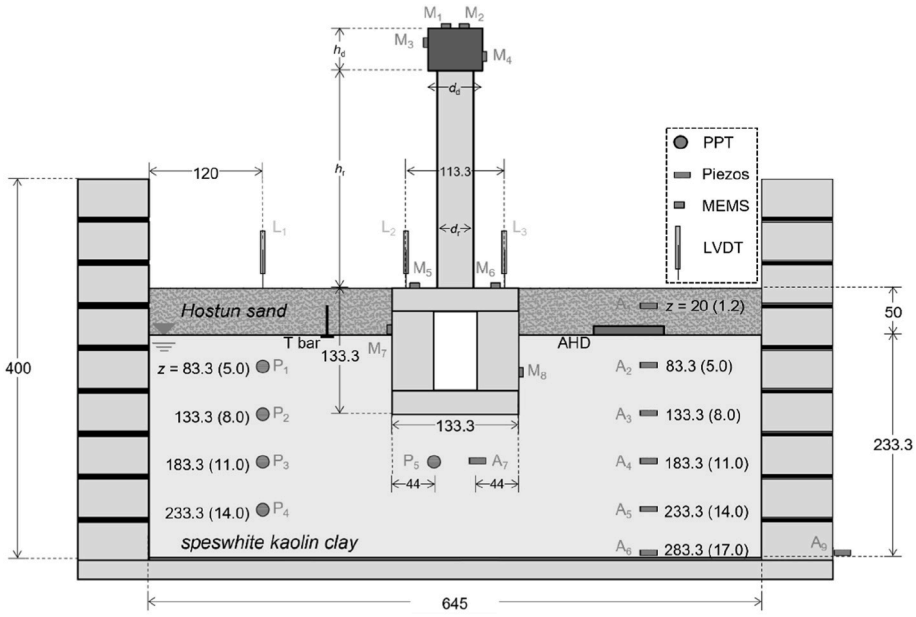

Fig. 3. Cross section view of the centrifuge model at model scale (in mm) (bracketed prototype dimensions in m).

Table 6
Properties of the speswhite kaolin clay adopted in the dynamic centrifuge tests [32].

w_L (%)	w_P (%)	PI	G_s (−)	Γ (−)	λ (−)	κ (−)	M (−)
58	34	24	2.61	2.87	0.14	0.03	0.80

experimental data as:

$$G_0(z_i) = \rho \cdot V_{S0}(z_i) \tag{1}$$

where ρ is the soil mass density and V_{S0} is the small-strain shear wave velocity obtained from the propagation time of the shear wave between two successive piezoelectric accelerometers.

The undrained shear strength was computed as:

$$s_u(z) = \frac{q_c(z)}{N_T} \tag{2}$$

where q_c is the measured penetration resistance and $N_T = 12$ is the bearing factor of the T-bar, which was calibrated against shear vane tests carried out after the experiment at 1*g* [11]. Fig. 4c and d shows the experimental profiles of G_0 and s_u for the two models. The profiles of G_0 measured for the two models are almost the same whereas the undrained shear strength of clay layer in test DG01 was about twice that of the clay layer in test DG02. This should not affect the comparison of the seismic behaviour of the rigid and flexible systems, as soil shear strength was never triggered during the earthquakes applied to the model, as clarified in the following.

The experimental strength and stiffness profiles were compared to those computed using empirical relations available in the literature. As for the small-strain stiffness profile, the formula proposed by Azeiteiro et al. [36] was adopted for the sand layer at the relative density measured in the experiment, $D_R = 50$ %, whereas those by Hardin and Drnevich [37] and Viggiani and Atkinson [38] were used for the clay stratum. The experimental undrained shear strength profiles were

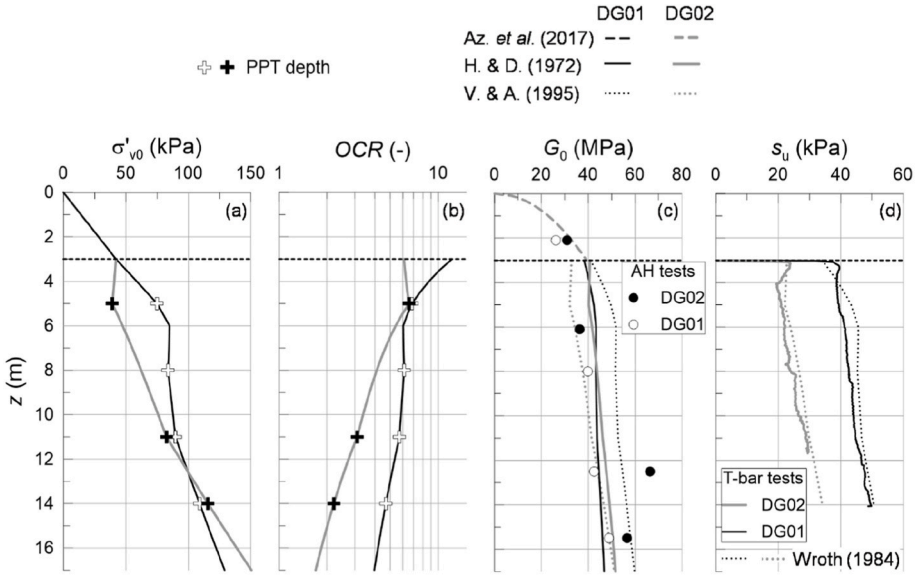

Fig. 4. (a) Vertical effective stress, (b) overconsolidation ratio, (c) small-strain shear modulus and (d) undrained shear strength profiles.

compared to the empirical relation by Wroth (1984):

$$s_u(z) = k \cdot \sigma'_{v0}(z) \cdot R_0^{\Lambda}(z) \quad (3)$$

where $k = 0.11 + 0.0037 \bullet PI = 0.1988$ [39], $R_0 = p'_{max}/p'$ is the 3D overconsolidation ratio, with p'_{max} and p' being the consolidation and current mean effective stress, respectively, and $\Lambda = (\lambda\text{-}\kappa)/\lambda = 0.79$, see Table 6. In all cases, the empirical predictions are in reasonable agreement with the experimental values, with the equation by Hardin and Drnevich [37] corresponding better with the profile of G_0 for both models. This clearly indicates that the state of vertical effective stress, σ'_{v0}, and the profile of overconsolidation ratio, *OCR*, given in Fig. 4a and b, were estimated correctly, due to the recording of excess pore water pressures, Δu, at some depth in the clay stratum, corresponding to the crosses in Fig. 4a and b. Excess pore water pressures in the clay had not fully dissipated before the input motions were applied to the models, as the in-flight consolidation following the spin-up process, carried out in steps of 10*g*, did not last enough, as indicated by the recordings of the PPTs.

Table 7 gives the average values of G_0 and s_u in the two tests, together with the estimate of the small-strain fundamental period of the soil column, T_0, estimated in the simplifying assumption of homogeneous soil:

$$T_0 = 4h \cdot \sum_{i=1}^{17} \frac{1}{V_{S0,i}} \quad (4)$$

where $h = 1$ m is the thickness of each of the seventeen sublayers in which the soil layer was subdivided. Because the soil stiffness profiles in the two models are very similar, almost identical values of the fundamental period were computed for tests DG01 and DG02, $T_0 = 0.43$ and 0.42 s, respectively.

3.2. Base excitations

The two models were subjected to the same series of nine base excitations, which were imposed at the base of the ESB container through the servo-hydraulic shaker available at the Schofield Centre [40]. The input seismic excitations are listed in the order they were applied in Table 8, which also reports the peak acceleration $a_{max,inp}$ of each input signal.

The applied ground motions reproduce both scaled real records and theoretical acceleration time histories, such as sinesweeps and trains of sinusoidal waves. Their amplitude was designed to be sufficient to promote the shear modulus decay required to observe period lengthening while not enough to trigger irreversible deformation in the soil, thus focusing only on the changes of fundamental period in the quasi-elastic regime. Finally, the sequence in which the seismic inputs were applied was selected to be able to check, while performing the centrifuge tests, the seismic-induced increase of the period T_{eq} with respect to the preceding one. As an example, BE_1 and BE_4 (low-intensity sinesweeps) were selected to observe the change in T_{eq} after applying BE_2 and BE_3 (Adana ground motion). Because the applied time histories were mostly low to moderate amplitude, it is likely that they would have had a limited effect on the soil state, which may otherwise have influenced the response of the system when subject to the following base excitations.

In some cases, the peak acceleration was not the same in the two tests: however, differences were almost always less than 20 %, except for BE_8 and 9, for which the maximum acceleration was very small.

Table 7
Main average mechanical properties of the soil column.

test	G_0 (MPa)	T_0 (s)	s_u (kPa)
DG01	41.2	0.43	43.3
DG02	42.7	0.42	24.1

Table 8
Base excitations applied in the centrifuge tests.

base excitation	ground motion	$a_{max,\ inp}$ (g)	
		DG01	DG02
BE_1	sinesweep	0.049	0.052
BE_2	Adana	0.119	0.105
BE_3	Adana	0.133	0.156
BE_4	sinesweep	0.051	0.053
BE_5	Christchurch	0.100	0.088
BE_6	Tolmezzo	0.106	0.104
BE_7	Kobe	0.209	0.212
BE_8	sine wave	0.120	0.059
BE_9	sine wave	0.017	0.005

To provide an indication of the frequency content of the applied seismic excitations, Fig. 5 shows their dimensionless Fourier amplitude spectra. Due to soil nonlinear behaviour, during the applied earthquakes, the fundamental frequency of the systems spanned in the range from $f_s = 1/T_s = 2.0$ Hz to $f_{eq,min} = 1/T_{eq,max} = 1.1$ Hz for test DG01, and $f_s \approx 1.1$ to $f_{eq,min} = 0.7$ Hz for DG02. To highlight potential resonance between the systems and the input motion, these ranges of fundamental frequency are indicated in Fig. 5. The issue of potential resonance, together with its role on the seismic performance of the systems, is discussed in the following.

4. Experimental behaviour of the systems

Fig. 6 shows the peak horizontal accelerations recorded in the far-field (a), on the top of the caisson (b), and at deck level (c) against the peak input acceleration, $a_{max,inp}$. The far-field accelerations obtained in the two tests (Fig. 6a), DG01 and DG02, are quite similar, and correspond to a mild amplification of the signal (*i.e.,* dots laying close to the 1:1 line), with a maximum amplification $r = a_{max,\ ff}/a_{max,\ inp} = 1.5$ and a minimum $r = 0.9$ being obtained for the base excitations BE_3 (Adana ground motion) and BE_6 (Tolmezzo ground motion), respectively. BE_9 was not considered in the computation of r due to its very low peak acceleration in test DG02 (Table 8). Based on the above, it is possible to conclude that: (i) the different flexibility of the structures in tests DG01 and DG02 did not affect the results, demonstrating that the far-field arrays are indeed far-field; (ii) the shear strength of the soil was not attained during wave propagation, or else the results would have been affected by the very different values of s_u in the two models; and (iii) because the two models have almost the same soil stiffness, G_0, any difference in their behaviour can be attributed to the different flexibility of the two piers.

The two tests also provided quite similar values for the peak caisson acceleration (Fig. 6b): this is because the dynamic properties of the clay deposit are similar in the two tests, and the caisson size and stiffness are the same. It follows that the effects of kinematic interaction in the two tests are similar, which permits to isolate the inertial interaction effects on the seismic performance of the systems. As expected, the peak accelerations measured at deck level are different (Fig. 6c), with those experienced by the flexible pier (test DG02) on average lower than those recorded on the rigid pier (DG01), *e.g.*, a difference $\Delta a_{max,\ d} \approx 0.1g$ at $a_{max,\ inp} \approx 0.21g$ (BE_7). However, for $a_{max,inp} \approx 0.05g$, higher pier accelerations were recorded for the flexible system of test DG02. This may be due to resonance of the flexible pier occurring for specific ground motions, namely sinesweeps BE_1 and BE_4 and sine wave BE_8 (see Fig. 5).

The seismic performance of the systems is evaluated here using some indices, such as the peak and permanent deck drift ratio, u_{rel}/h_s, and the peak bending moment applied at the top of the caisson by the pier, M; these are plotted in Fig. 7 as a function of the peak input acceleration, $a_{max,inp}$. Overall, the flexible pier experienced higher peak drifts due to its flexibility, even neglecting the three outliers attributed to resonance at $a_{max,\ inp} \approx 0.05g$: the maximum peak deck drift ratio was equal to

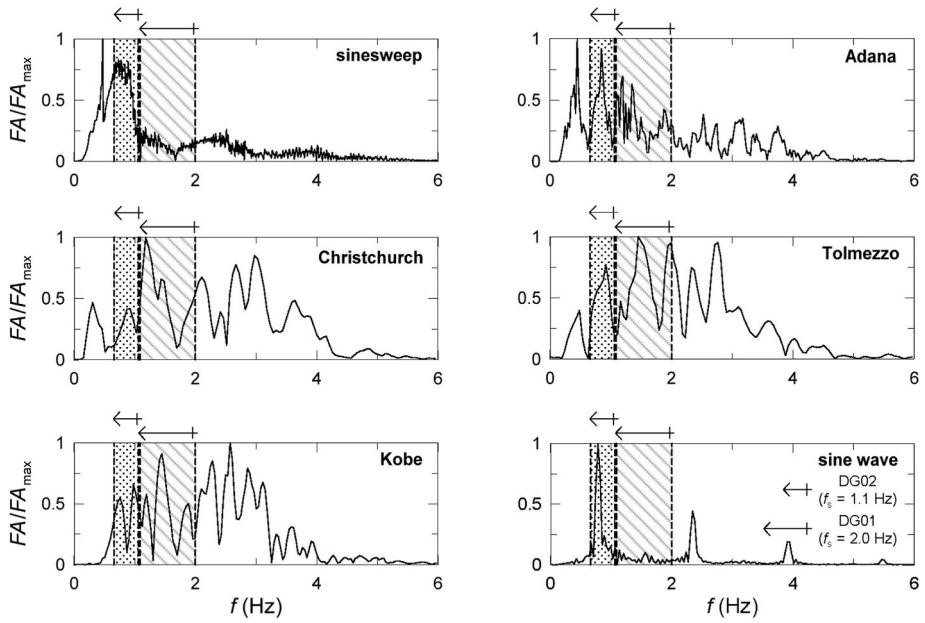

Fig. 5. Dimensionless Fourier amplitude spectra of ground motions (at prototype scale) with shaded areas indicating the frequency range spanned by the system during the tests.

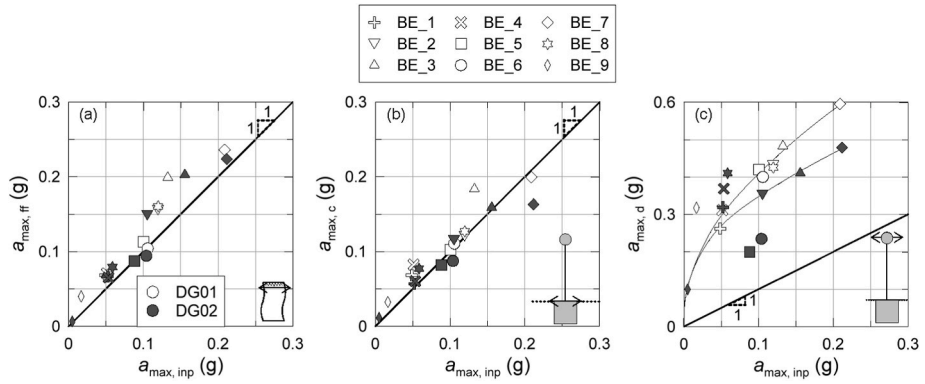

Fig. 6. Peak accelerations recorded at the: (a) far-field ground surface; (b) top of the caisson; (c) deck level.

about 15 and 11 ‰ for the flexible and rigid system indeed, both attained for the highest-intensity base excitation considered in the study (BE_7). On the other hand, similar values of permanent drift (Fig. 7b) and peak bending moment (Fig. 7c) were recorded for the two systems. The small values of permanent deck drift, always less than 1 ‰, testifies that soil plastic strains were not attained during shaking and that its behaviour may be assumed as nonlinear elastic for the cases at hand, as further discussed in the following. As for the peak bending moment, an almost identical peak value was computed ($M_{max} \approx 25$ MN m for BE_7), although different peak deck accelerations were recorded for the two systems ($a_{max,\ d} = 0.60$ and 0.48 g for the rigid and flexible system, respectively), which is to be attributed to the different mass of the

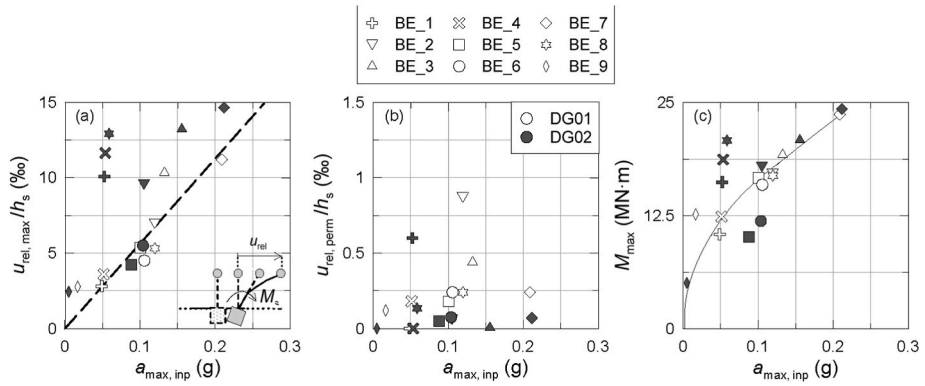

Fig. 7. (a) Peak and (b) permanent deck drift ratio; (c) peak moment atop the caisson vs. peak input acceleration.

equivalent SDoF, $m_s = m_d + 1/2 \bullet m_p$ (=266.2 Mg and 319.1 Mg for the rigid and flexible system, respectively).

Fig. 8 shows the time histories of total drift, rocking drift, and bending moment transmitted by the pier at the top of the caisson for base excitation BE_6 (Tolmezzo). The rigid component of the total deck drift is proportional to the tangent of the rigid rotation of the caisson foundation, tanθ. A slightly larger total drift was recorded for the flexible pier (DG02, black line), with a value of 5.50 against 4.50 ‰, whereas a larger rigid drift was recorded for the rigid pier (DG01, grey line). While the total drift may be ascribed to the flexibility of the pier, the rigid drift may be attributed to the slightly higher peak bending moment experienced by the stiffer pier (15.93 MNm vs. 11.92 MNm). For the same base excitation, the soil-foundation response is given in Fig. 9a and b in terms of moment-rotation, M - θ, and relative settlement-rotation, ($w - w_{ff}$) - θ, loops. The caisson of the rigid system (DG01) underwent a peak rotation which was almost twice that experienced by the caisson supporting the flexible pier (0.19 % vs. 0.10 %). Therefore, the average, secant soil-foundation stiffness for the rigid system is about half that of the flexible system, as the two caissons experienced a similar peak moment. Here it is worth mentioning that the caisson foundation was actually subjected to additional contribution of moment, such as those caused by the rotational inertia of the pier tip and caisson mass [41]: however, these contributions were not included here as they were about 0.1 and 8 % of the one resulting for the rigid and flexible pier, respectively. Moreover, very low permanent relative settlements were recorded for both systems, namely $w - w_{ff} = 3.5$ vs. 1.0 mm (=0.04 and 0.01 % of the caisson diameter) for the rigid and flexible system, respectively, which confirms the almost purely reversible soil behaviour involved during the centrifuge tests (Fig. 9b).

From the foregoing it follows that a higher soil shear modulus decay was attained for the rigid system (DG01) over the seismic event, which increased soil-caisson compliance and, in turn, the fundamental period of the system with respect to the fixed-base one, as it will be discussed in the following section (§ 5).

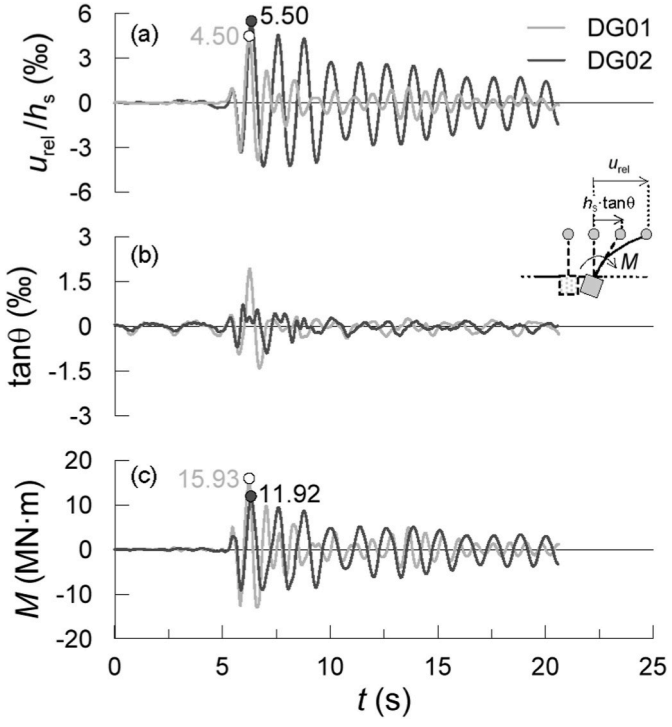

Fig. 8. Time histories of the (a) total and (b) rocking drift, and (c) moment atop the caisson for BE_6.

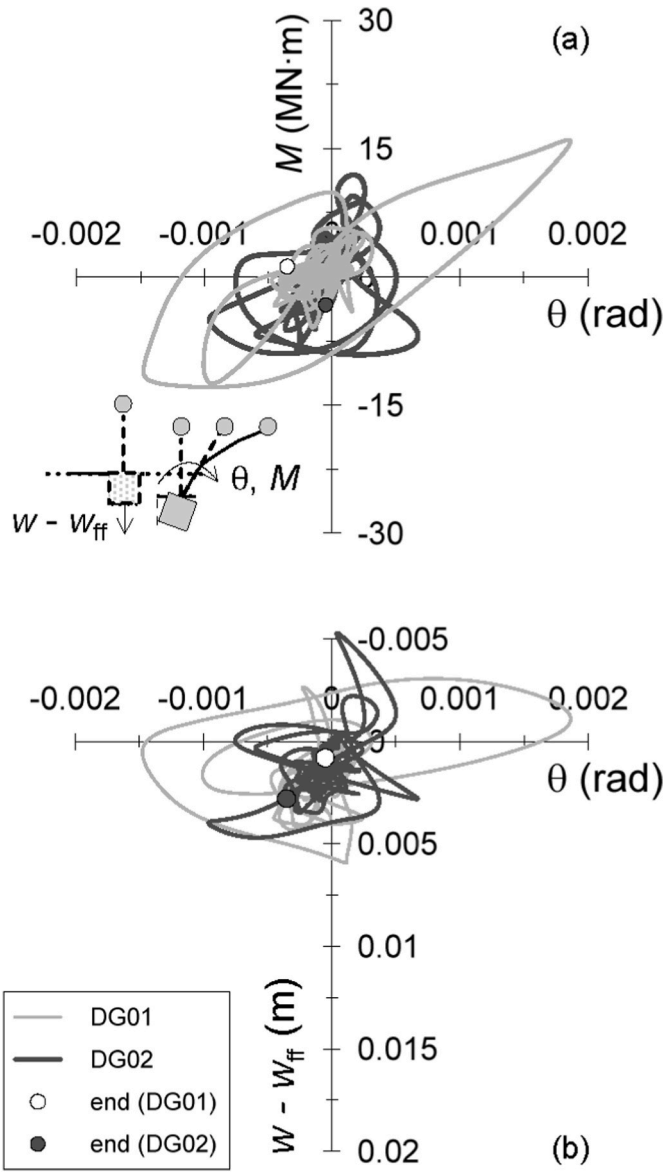

Fig. 9. (a) Moment and (b) settlement-rotation loops experienced by the caisson for BE_6.

4.1. Computation of the compliant-base period

The fundamental compliant-base period of the systems, T_{eq}, was computed as the period for which the maximum ratio of the elastic acceleration spectra recorded at deck level to the far-field ground surface (piezo A1 in Fig. 3) was attained. An example is provided in Fig. 10 for both systems subjected to base excitation BE_6: values $T_{eq} = 0.77$ and 1.29 s were obtained for the rigid and flexible system, respectively. Table 9 summarises the values obtained for all base excitations; note that the average of all the periods ($T_{eq,\,ave} = 0.76$ s for the rigid and 1.36 s for the flexible system) are almost coincident with those measured from the free-oscillations induced by a horizontal impact at deck level after swing down, $T_{eq} = 0.75$ s and 1.36 s for the rigid (DG01) and flexible (DG02) system, respectively.

The different fundamental periods of the rigid and flexible piers were responsible for the different seismic performance of the two systems, shown in Figs. 11 and 12 in terms of spectral acceleration at deck level, *S*a, and spectral displacement, *S*d, for base excitations BE_6 (Tolmezzo) and BE_3 (Adana). Spectral values were normalised with respect to the peak input acceleration because of the slightly different applied values

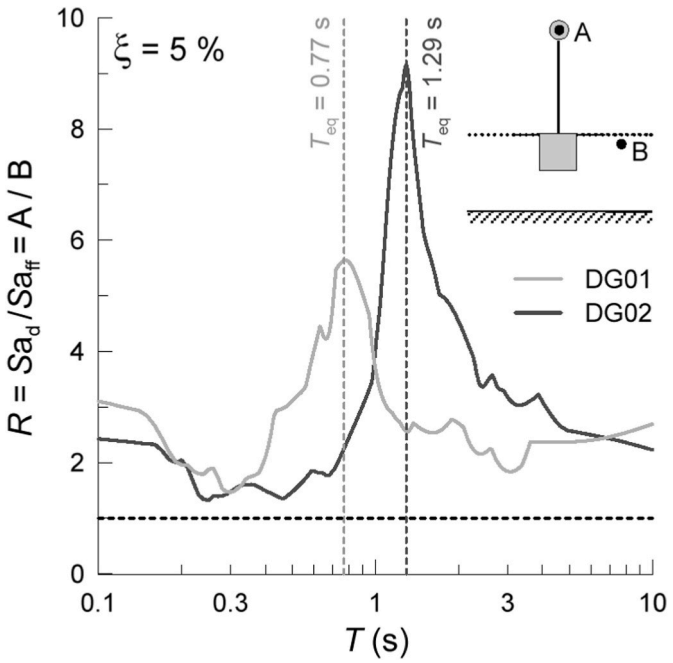

Fig. 10. Deck-to-far-field spectral ratios adopted to compute the equivalent period of the systems for BE_6.

of $a_{max,inp}$ in the two tests (Table 8). The maximum acceleration and displacement experienced by the systems plot very closely to the elastic response spectra of the acceleration time histories recorded at ground surface in the far field, as expected. The far-field spectra were computed for the damping ratio of compliant-base structures, $\xi_{eq} = 2.2$ %, which was similar for the two systems from the free-oscillations of impact hammer tests performed after the centrifuge test. The slight deviation of the peak values experienced by the structures from the spectral ones may be attributed to some kinematic interaction effects, as well as possible inaccuracy in estimating the damping ratio of the system. Nonetheless, it is apparent that the higher the fundamental period, the higher the displacements and the lower the accelerations experienced by the structure, which is a characteristic of slender structures which are on the descending tail of the acceleration spectra, when high-period seismic inputs are not anticipated. It is also interesting to notice that, although the two systems are characterised by quite different periods T_{eq}, they underwent almost the same peak deck acceleration when subjected to BE_3, which is a direct consequence of the symmetry of the relevant spectrum (Fig. 12a). The results possess the added value of having been obtained experimentally, showing how the compliant-base period T_{eq} plays a key role in the seismic performance of such structures.

The period T_{eq} was also observed to be a function of $a_{max,inp}$ (Fig. 13a). The fundamental period increases with $a_{max,inp}$ for both systems, ranging between 0.68 and 0.92 s for the relatively rigid system (DG01 test) and between 1.20 and 1.52 s for the relatively flexible system (DG02). The increase with the input acceleration can be ascribed to the nonlinear soil behaviour, *i.e.*, shear modulus decaying with increasing seismic intensity. The period lengthening is therefore quantified in terms of the ratio T_{eq}/T_s (Fig. 13b), which expresses the increase of the period of the system with respect to the fixed-base system. The ratio ranges between 1.36 and 1.84 for the rigid pier and 1.28 and 1.62 for the flexible pier. As expected from the analytical solutions available in the literature, the period lengthening is more evident for the rigid system than for the flexible one. This result conforms to the concept of soil-to-structure stiffness ratio, usually expressed in the literature by the dimensionless wave parameter σ [42], which can be rearranged as

Table 9
Experimental equivalent period of the system.

base excitation	DG01				DG02			
	$T_{eq,\ exp.}$ (s)	$T_{eq,\ emp.}$ (s)	$V_{S,\ eq}$ (m/s)	$T_{eq,\ emp.}/T_{eq,\ exp}$	$T_{eq,\ exp.}$ (s)	$T_{eq,\ emp.}$ (s)	$V_{S,\ eq}$ (m/s)	$T_{eq,\ emp.}/T_{eq,\ exp}$
BE_1	0.68	0.70	115.22	1.03	1.41	1.15	109.38	0.82
BE_2	0.69	0.78	88.57	1.12	1.34	1.23	85.81	0.91
BE_3	0.69	0.81	80.49	1.17	1.34	1.28	74.66	0.95
BE_4	0.75	0.70	116.02	0.93	1.40	1.15	111.47	0.82
BE_5	0.78	0.71	112.77	0.91	1.27	1.15	110.84	0.91
BE_6	0.77	0.73	102.76	0.95	1.29	1.18	98.65	0.92
BE_7	0.92	0.88	67.23	0.96	1.44	1.35	63.29	0.94
BE_8	0.86	0.79	84.25	0.92	1.52	1.21	90.33	0.80
BE_9	0.69	0.66	142.90	0.95	1.20	1.09	149.52	0.91

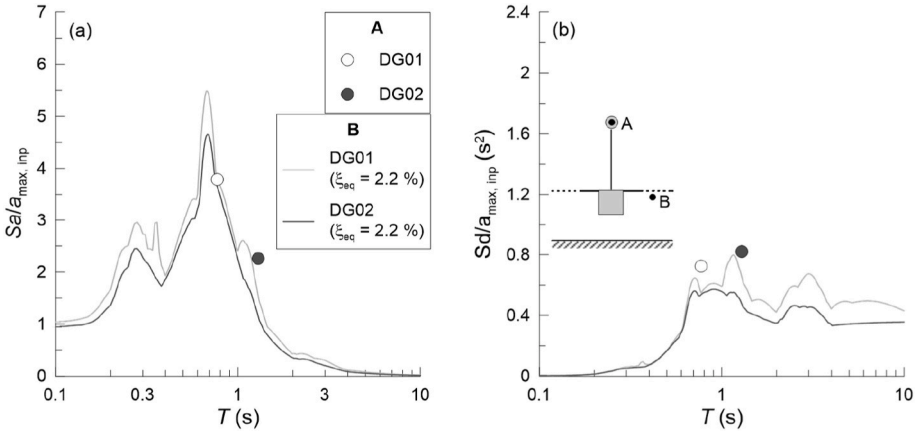

Fig. 11. Elastic (a) spectral acceleration and (b) displacement at the far-field ground surface normalised to the peak input acceleration, compared to peak deck acceleration and displacement obtained for BE_6.

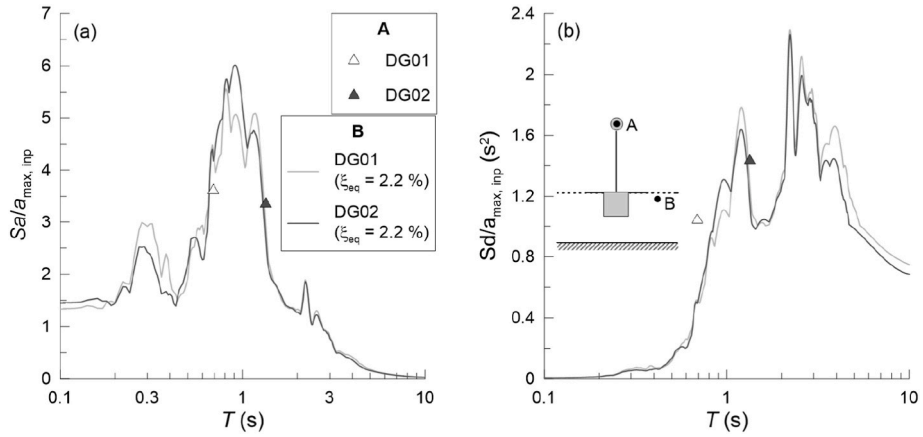

Fig. 12. Elastic (a) spectral acceleration and (b) displacement at the far-field ground surface normalised to the peak input acceleration, compared to peak deck acceleration and displacement obtained for BE_3.

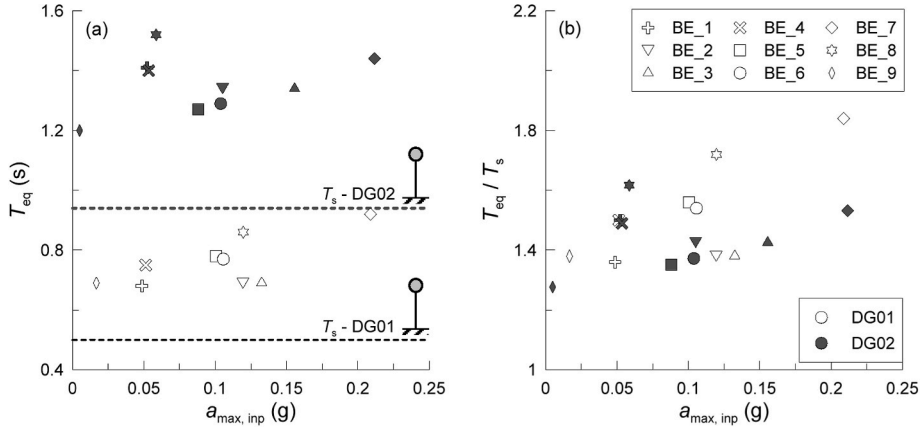

Fig. 13. (a) Equivalent period and (b) period lengthening against the peak input acceleration.

$$\sigma = \frac{V_{S,eq} \cdot T_s}{h_s} \tag{5}$$

where $V_{S,eq}$ is the equivalent shear wave velocity of the soil deposit. Period lengthening is maximum when σ tends to 0, which means relatively soft soils compared to the structure. Furthermore, as T_s and h_s are constant for a given system, the influence of seismic intensity on the period lengthening will be included in $V_{S,eq}$. The wave parameter in eq. (5) was proposed for a shallow and rigid footing and therefore does not consider the embedment of the foundation. Therefore, an additional parameter taking into account the embedment of the caisson, H, is needed, as discussed in the next section.

5. Comparison with relationships available in the literature

Previous paragraphs showed that the equivalent, compliant-base period of the system, T_{eq}, may be well correlated to the seismic performance of the systems at hand. Therefore, it is of interest to investigate whether the experimental equivalent period obtained in the centrifuge tests may be estimated reliably from empirical relationships already available in the literature.

The empirical relation by Tsigginos *et al.* [25] was developed based on 3D Finite Element numerical analyses of caisson foundations supporting bridge piers:

$$T_{eq} = T_s \cdot \left[1 + \left(\frac{2\pi}{\sigma}\right)^{1.18} \left(\frac{m_s}{m_c}\right)^{0.613} \left(2\frac{h_s}{D}\right)^{-0.5}\right] \tag{6}$$

where: m_s is the tip mass of the SDoF oscillator equivalent to the superstructure; m_c is the mass of the caisson, proportional to the foundation embedment H; and $V_{S,eq}$ is the equivalent shear wave velocity in the zone of influence of the foundation, here assumed to extend to a maximum depth $z_{max} = H + D = 16$ m. $V_{S,eq}$ is related to the shear modulus, G, mobilised during the earthquake, which decays with the shear strains applied by the travelling S-waves to the soil column, which in turn depend on the seismic intensity.

The equivalent shear wave velocity $V_{S,eq}$ was computed from 1D Site Response Analyses (SRAs) performed with the Linear Equivalent (LE) method [43] using the code MARTA [44], for all base excitations applied in the centrifuge tests. In the analyses, the soil behaviour was described as non-linear viscous-elastic, which was assumed thanks to the evidence of almost no plastic soil response, which provided very low permanent drifts and settlements of the system (Figs. 7b, 8b and 9b). The analytical G_0 profile by Hardin and Drnevich [37] was adopted for the clay, for both the DG01 and DG02 tests (Fig. 4c); as for the shear modulus decay ($G/G_0(\gamma)$) and damping increase ($\xi(\gamma)$) with the shear strain, the curves by Darendeli [45] were adopted both for the sand and the clay layer, also taking into account the different initial stress state recorded in the two tests DG01 and DG02 (see Fig. 4a).

Fig. 14 shows the results of the 1D SRAs performed for the profiles of G_0 shown in Fig. 4c. For the sake of brevity, here only the results for the DG01 profile are discussed, as those for DG02 are very similar. The results are given in terms of profiles of peak acceleration ratio, $r = a_{max}/a_{max,\ inp}$, peak shear strain, γ_{max}, shear modulus decay, G/G_0, and "mobilised" shear wave velocity $V_S = \sqrt{G/\rho}$, for all seismic inputs. The

equivalent shear wave velocity $V_{S,eq}$ was calculated as

$$V_{S,eq} = \frac{\sum_{i=1}^{16} h}{\sum_{i=1}^{16} \frac{h}{V_{S,i}}} = \frac{H+D}{\sum_{i=1}^{16} \frac{h}{V_{S,i}}} \tag{7}$$

where $V_{S,i}$ is the average shear wave velocity of the i^{th} sublayer. The values of $V_{S,\,eq}$ obtained are listed in Table 9, together with the relevant period T_{eq} obtained with Equation (6) and the comparison with the experimental result, which exhibits a maximum difference of about 20 %.

The outcomes of the procedure are also plotted in Fig. 15, both in terms of the equivalent period T_{eq} (a) and the period lengthening, represented by the ratio T_{eq}/T_s (b). It is evident that the agreement is good, which shows that preliminary 1D LE SRAs may be profitably carried out to take into account the influence of seismic intensity on the equivalent period T_{eq}, which are related through the nonlinear soil behaviour.

The results discussed above are further confirmed following the same procedure as that described by De Angelis *et al.* [16]. To this end, the ratio K_{eq}/k_s was computed for both systems and all base excitations ($2 \times 9 = 18$ cases), where K_{eq} is the equivalent, overall stiffness of the soil-caisson-pier system, and k_s is the flexural stiffness of the fixed-base pier. The experimental ratio was computed as

$$\left\{\frac{K_{eq}}{k_s}\right\}_{exp.} = \left(\frac{T_{eq}}{T_s}\right)^{-2} \tag{8}$$

while the analytical ratio was computed adopting $k_s = \omega_s^2 \cdot m_s$, with $\omega_s = 2\pi/T_s$, and the following equation for the overall stiffness, K_{eq}:

$$\left\{\frac{K_{eq}}{k_s}\right\}_{an.} = \left\{\frac{k_s}{K_{xx}} + k_s \cdot \frac{\left[(H+h_s) - \frac{K_{xr}}{K_{xx}}\right]^2}{\left[K_{rr} - \frac{K_{xr}^2}{K_{xx}}\right]} + 1\right\}^{-1} \tag{9}$$

where the soil-caisson translational, K_{xx}, coupled, K_{xr}, and rotational, K_{rr}, dynamic stiffnesses were computed at the base of the caisson (depth $z = H$) for the experimental circular frequency $\omega_{eq} = 2\pi/T_{eq,\,exp.}$ with the expressions provided by Gazetas [18] for a homogenous, linear viscous-elastic stratum over bedrock, characterised by a constant mobilised shear modulus, $G = \rho \cdot V_{S,\,eq}^2$, with $V_{S,\,eq}$ from Table 9 (varying with the base excitation). The results are plotted in Fig. 16. The comparison of the experimental results with the analytical ones is good, with most of the points falling in the shaded area detected by De Angelis *et al.* [16]. This gives confidence in the analytical relationship by Gazetas [18] used to compute the dynamic stiffness. As already noticed for the equivalent period T_{eq} (Fig. 15), the rigid system turned out to be slightly stiffer than predicted by the analytical relationship (*i.e.*, higher equivalent stiffness, K_{eq}), whereas the flexible one showed a slightly lower equivalent stiffness than predicted. These deviations may be attributed to the cases considered in the centrifuge not matching exactly those taken into account in De Angelis *et al.* [16]. For instance, cylindrical caissons with an aspect ratio of the caisson cross section equal to one were simulated in the present study, whereas De Angelis *et al.* [16] examined aspect ratios ≥ 3.

6. Practical implications for design

The seismic performance of critical infrastructure, such as bridge piers on caisson foundations, can be assessed in the framework of Performance-Based Design (PBD). As caissons are typically adopted for tall piers, *i.e.*, flexible structures, radiation damping is quite low [46]. Hence, the equivalent fundamental period is the main dynamic parameter governing the seismic performance of such systems.

From the experimental study and its interpretation discussed above, some general practical implications may be derived for the seismic design of caisson foundations supporting bridge piers, provided that the seismic intensity is such that the soil behaviour may be adequately simulated as linear viscous-elastic, which is typically the case for $\gamma_{max} \leq$ 0.2–0.3 %.

- increase from the fixed-base to the compliant-base period may be significant and may be successfully taken into account performing preliminary SRAs with the LE method to assess the peak accelerations and permanent tilt of the structure;
- the equivalent period T_{eq} may be initially estimated using the empirical relationships available in the literature, such as that by Tsigginos *et al.* [25], as demonstrated above, or by Zania [24]. Alternatively, the equivalent period may be successfully computed by building simplified LPM models of the whole structure, where the superstructure is modelled through a SDoF oscillator resting on selected dynamic impedances, such as those proposed by Gazetas [18] for $H/D \leq 1.5$ and Varun *et al.* [1] for $H/D \geq 2$, which add to those by Pais and Kausel [17], Mylonakis *et al.* [19] and Carbonari *et al.* [20]. More details on this approach are given in De Angelis *et al.* [16], Conti and Di Laora [47] and Gaudio and Rampello [48].

Whether adopting empirical relations or based on dynamic impedances, mobilised values of the soil shear modulus G are to be adopted. As this modulus is a decreasing function of the mobilised shear strain γ, which in turn is a function of seismic intensity, preliminary 1D free-field ground response analyses should be performed; in the simplest form,

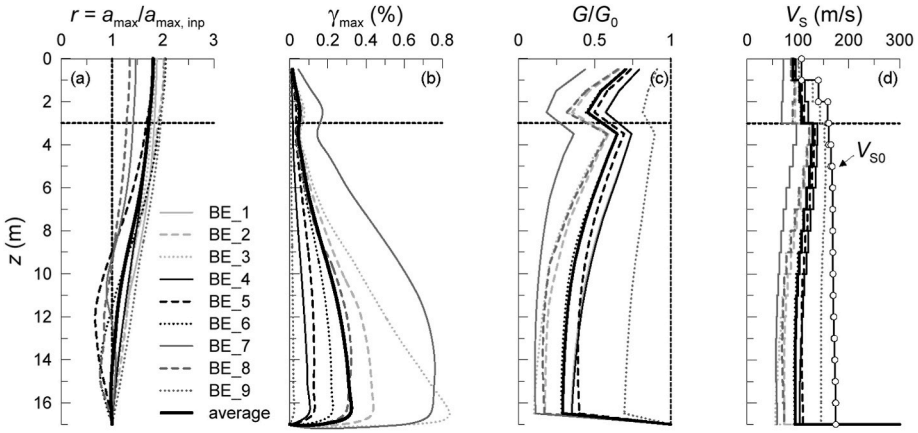

Fig. 14. Main results of 1D SRAs reproducing the DG01 soil column. Profiles of (a) peak acceleration ratio; (b) peak shear strain; (c) shear modulus decay and (d) mobilised shear wave.

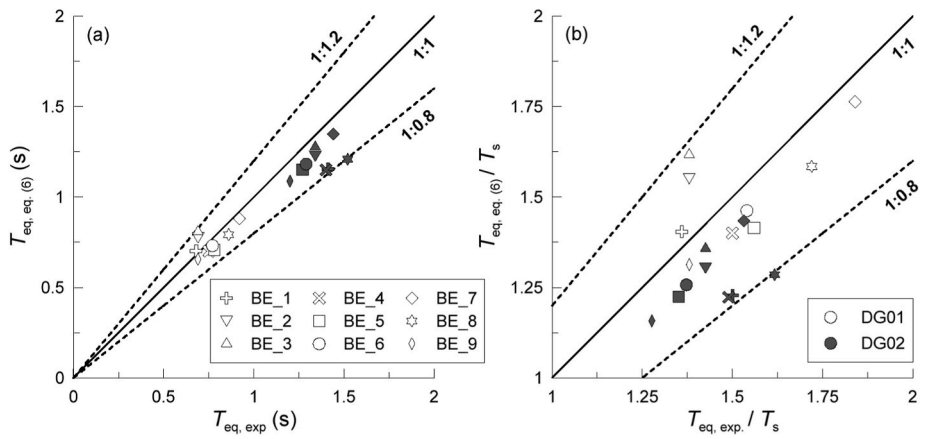

Fig. 15. Comparison of the (a) compliant-base period and (b) period lengthening from the centrifuge and from the semi-empirical equation by Tsigginos et al. [25] with the mobilised shear wave velocity from 1D LE SRAs.

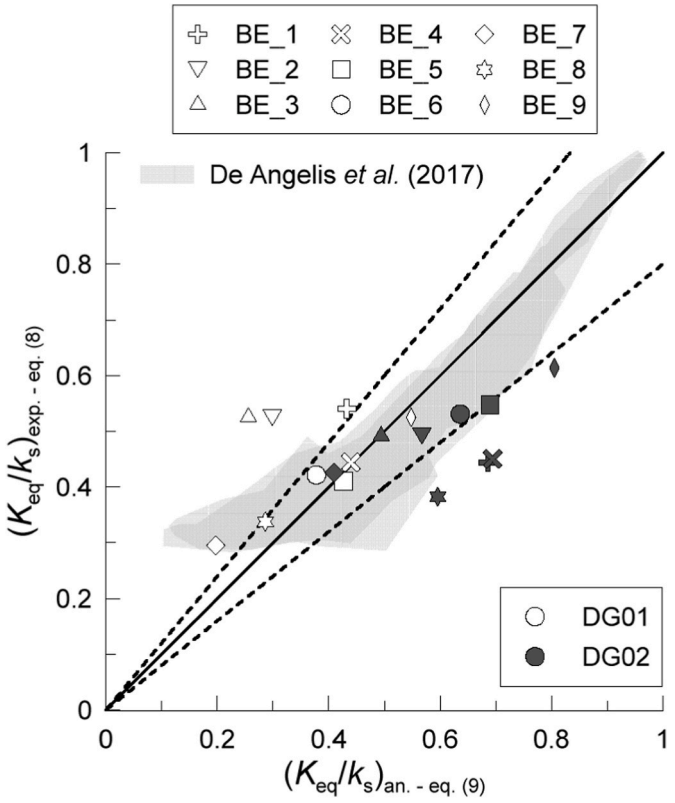

Fig. 16. Comparison of the normalised equivalent stiffness from the centrifuge and theoretically with the soil-caisson dynamic stiffnesses by Gazetas [18] with the mobilised shear wave velocity from 1D LE SRAs.

these may be carried out using the Linear Equivalent (LE) method [43]. Here it is worth noting that time-frequency analyses (*e.g.*, Stockwell transform [49]) should have been carried out to be rigorous, as the fundamental period is changing over the earthquake. However, since the range of the maximum shear strain underwent by the soil for the cases at hand is below the above-mentioned threshold of 0.3 % for the depths of interest (up to $z = H + D = 16$ m), the fundamental period can be still computed following a linear-equivalent procedure. Conversely, in the presence of higher-intensity seismic input the elasto-plastic soil behaviour would be involved, eventually involving soil shear strength and the bearing capacity of the caisson. Under these circumstances, the increase of the system fundamental period may still occur, although at a lower and lower rate. Nonetheless, detecting the fundamental period in the deep plastic regime would become more challenging, thus requiring time-frequency analyses to be performed.

7. Concluding remarks

The topic of caisson foundations supporting bridge piers subjected to strong earthquakes has been attracting the interests of researchers in recent years. The seismic performance of the systems is assessed routinely through simplified methods where the fundamental, compliant-base period constitutes one of the main input parameters. Several analytical and empirical relations are already available in the literature for this purpose: however, shortage of field monitoring of such structures makes experimental investigation of reduced-scale models of primary importance to validate these expressions and relevant theoretical findings.

In this paper, the results of an experimental investigation carried out through dynamic centrifuge testing, have been showed and discussed. Two different bridge piers, one rigid and the other flexible, on the same cylindrical caisson foundation, were subjected to a series of both sinusoidal and real motions, and the relevant seismic performance computed referring to indices typically adopted in the practice. The latter were first shown to strongly depend on the equivalent fundamental period of the system T_{eq}, which increase noticeably with respect to the fixed-base period T_s, particularly for the rigid system. Moreover, the equivalent period T_{eq} turned out to be a function of nonlinear (but still almost-entirely reversible) soil behaviour, that leads to the shear modulus decay during the seismic event, although neither the irreversible behaviour nor its shear strength was involved in the cases at hand. These two novel findings may be useful and have practical implications for design, since they come from experimental, dynamic centrifuge testing, which allowed emphasising the link between the equivalent period and the intensity of the seismic input.

The experimental equivalent period of the system was finally compared to the estimates that can be obtained from the empirical formula proposed by Tsigginos *et al.* [25]. It has been shown that a correct estimate of this parameter would need the shear modulus decay to be accounted for, by performing 1D site response analyses with the well-known Linear Equivalent Method, at least. This equation, now validated against experimental results, permits to determine the period lengthening due to the compliance of the soil-caisson system and, therefore, to understand whether dynamic soil-structure interaction effects are to be accounted for or if the fixed-base assumption may be deemed adequate, which is typically not the case in the presence of moderate-to-high-intensity ground motions.

It is worth noting that the equivalent period is not the only parameter

affecting the seismic performance of such structures: conversely, a mass parameter of the whole system should be added in the Authors' opinion, in order to better predict period lengthening on the seismic behaviour of caisson foundations supporting bridge piers.

Funding

The authors did not receive support from any organization for the submitted work.

CRediT authorship contribution statement

Domenico Gaudio: Conceptualization, Data curation, Investigation, Methodology, Validation, Writing – original draft, Writing – review & editing. **Gopal S.P. Madabhushi:** Methodology, Supervision, Writing – review & editing. **Sebastiano Rampello:** Conceptualization, Investigation, Supervision, Writing – review & editing. **Giulia M.B. Viggiani:** Conceptualization, Funding acquisition, Investigation, Methodology, Supervision, Writing – review & editing.

Declaration of competing interest

The authors declare that they have no known competing financial interests or personal relationships that could have appeared to influence the work reported in this paper.

Data availability

Data will be made available on request.

Acknowledgements

The centrifuge experiments were performed with the excellent help of technicians at the Schofield Centre of University of Cambridge. This support is gratefully acknowledged.

References

[1] Varun D Assimaki, Gazetas G. A simplified model for lateral response of large diameter caisson foundations - linear elastic formulation. Soil Dynam Earthq Eng 2009;29(2):268–91.
[2] Pauselli D, Salciarini D, Ubertini, F F. Three-dimensional modeling of soil-structure interaction for a bridge founded on caissons under seismic conditions. Appl Sci 2022;12(21):10904.
[3] Kumar M, Chatterjee K. Load-sharing behavior of caisson foundations in layered soil under seismic conditions. Int J GeoMech 2023;23(6):04023055.
[4] Kausel E, Whitman RV, Morray JP, Elsabee F. The spring method for embedded foundations. Nucl Eng Des 1978;48(2):377–92.
[5] Conti R, Di Laora R, Licata V, Iovino M, de Sanctis L. Seismic performance of bridge piers: caisson vs pile foundations. Soil Dynam Earthq Eng 2020;130:105985.
[6] Zafeirakos A, Gerolymos N. On the seismic response of under-designed caisson foundations. Bull Earthq Eng 2013;11(5):1337–72.
[7] Gaudio D, Rampello S. Dynamic soil-structure interaction of bridge-pier caisson foundations. In: Geotechnical engineering in multidisciplinary research: from microscale to regional scale CNRIG2016. VI Italian conf. Of researchers in geotechnical engineering, procedia engineering, vol. 158. Elsevier; 2016. p. 146–51.
[8] Gaudio D, Rampello S. The influence of soil plasticity on the seismic performance of bridge piers on caisson foundations. Soil Dynam Earthq Eng 2019;118:120–33. https://doi.org/10.1016/j.soildyn.2018.12.007.
[9] Gazetas G. 4th Ishihara lecture: soil-foundation-structure systems beyond conventional seismic failure thresholds. Soil Dynam Earthq Eng 2015;68:23–39.
[10] Pecker A. Development of the second generation of Eurocode 8-part 5: a move towards performance-based design. In: *Earthquake geotechnical Engineering for Protection and Development of Environment and constructions*, silvestri & moraci; 2019. p. 273–81. 7th *Int. Conf. Earthq. Geotech. Eng.*-7ICEGE Rome 2019.
[11] Gaudio D, Madabhushi SPG, Rampello S, Viggiani GMB. Experimental investigation of the seismic performance of caisson foundations supporting bridge piers, vols. 1–16. Géotechnique, Thomas Telford Ltd; 2022. ISSN: 0016-8505, https://www.icevirtuallibrary.com/doi/abs/10.1680/jgeot.22.00076.
[12] Gerolymos N, Zafeirakos A, Karapiperis K. Generalized failure envelope for caisson foundations in cohesive soil: static and dynamic loading. Soil Dynam Earthq Eng 2015;78:154–74.
[13] Rosati A, Gaudio D, di Prisco C, Rampello S. Use of interaction domains for a displacement based design of caisson foundations. Acta Geotechnica 2023;18(1): 445–68. ISSN: 1861-1125, https://link.springer.com/article/10.1007/s11440-022-01547-z.
[14] Piro A, de Silva F, Parisi F, Scotto di Santolo A, Silvestri F. Effects of soil-foundation-structure interaction on fundamental frequency and radiation damping ratio of historical masonry building sub-structures. Bull Earthq Eng 2020;18: 1187–212.
[15] Somma F, Bilotta E, Flora A, Viggiani GMB. Centrifuge modeling of shallow foundation lateral disconnection to reduce seismic vulnerability. J Geotech Geoenviron Eng 2022;148(2):04021187. ASCE.
[16] De Angelis A, Mucciacciaro M, Pecce MR, Sica S. Influence of SSI on the stiffness of bridge systems founded on caissons. J Bridge Eng 2017;22(8):04017045.
[17] Pais A, Kausel E. Approximate formulas for dynamic stiffnesses of rigid foundations. Soil Dynam Earthq Eng 1988;7(4):213–27.
[18] Gazetas G. Foundation vibrations. In: Foundation engineering handbook. Springer US; 1991. p. 553–93.
[19] Mylonakis G, Nikolaou S, Gazetas G. Footings under seismic loading: analysis and design issues with emphasis on bridge foundations. Soil Dynam Earthq Eng 2006; 26(9):824–53.
[20] Carbonari S, Bordón JDR, Padrón LA, Morici M, Dezi F, Aznárez JJ, Leoni G, Maeso O. Winkler model for predicting the dynamic response of caisson foundations. Earthq Eng Struct Dynam 2022;51:3069–96.
[21] Jennings PC, Bielak J. Dynamics of building - soil interaction. Bull Seismol Soc Am 1973;63(1):9–48.
[22] Wolf JP. Soil–structure interaction. New Jersey, USA: Prentice Hall; 1985.
[23] Maravas A, Mylonakis, G G, Karabalis DL. Simplified discrete systems for dynamic analysis of structures on footings and piles. Soil Dynam Earthq Eng 2014;61:29–39.
[24] Zania V. Natural vibration frequency and damping of slender structures founded on monopiles. Soil Dynam Earthq Eng 2014;59:8–20.
[25] Tsigginos C, Gerolymos N, Assimaki D, Gazetas G. Seismic response of bridge pier on rigid caisson foundation in soil stratum. Earthq Eng Eng Vib 2008;7(1):33–44.
[26] Vucetic M, Dobry R. Effect of soil plasticity on cyclic response. J Geotech Eng 1991; 117(1):89–107. ASCE.
[27] Madabhushi SPG. Centrifuge modelling for civil engineers. Boca Raton: Taylor & Francis Group; 2014.
[28] Adamidis O, Madabhushi SPG. Rocking response of structures with shallow foundations on thin liquefiable layers. Geotechnique 2022;72(2):127–45.
[29] Gaudio D, Seong J, Haigh SK, Viggiani GMB, Madabhushi SPG, Shrivatsava R, Veluvolu R, Padhy P. Boundary effects on dynamic centrifuge modelling of onshore wind turbines on liquefiable soils. Int J Phys Model Geotech 2023;23(1):16–34. https://doi.org/10.1680/jphmg.21.00085.
[30] Brennan AJ, Madabhushi SPG. Design and performance of a new deep model container for dynamic centrifuge testing. In: *Proc. Int. Conf. Phys. Mod. Geotech.*, balkema; 2002. p. 183–8. Rotterdam, The Netherlands, St Johns NF, Canada. 2002.
[31] Garala TK, Madabhushi SPG. Seismic behaviour of soft clay and its influence on the response of friction pile foundations. Bull Earthq Eng 2019;17(4):1919–39.
[32] Viggiani GMB. *Small strain stiffness of fine grained soils*. PhD dissertation. City University of London; 1992.
[33] Gaudio D, Rampello S. The role of soil constitutive modelling on the assessment of seismic performance of caisson foundations. In: *Earthquake geotechnical Engineering for Protection and Development of Environment and constructions*, silvestri & moraci. 7th *int. Conf. Earthq. Geotech. Eng.* - 7ICEGE Rome 2019. Taylor & Francis Group – CRC Press; 2019. p. 2574–82. 978-0-367-14328-2.
[34] Ghosh B, Madabhushi SPG. An efficient tool for measuring shear wave velocity in the centrifuge. In: Phillips R, Guo PJ, Popescu R, editors. Proc. Int. Conf. Phys. Mod. Geotech. Balkema; 2002. p. 119–24.
[35] Stewart DP, Randolph MF. A new site investigation tool for the centrifuge. In: *Proc. Int. Conf. Centr. Mod.*, centrifuge '91; 1991. p. 531–8. Boulder, Colorado, Balkema, the Netherlands.
[36] Azeiteiro RJN, Coelho PALF, Taborda DMG, Grazina JCD. Critical state-based interpretation of the monotonic behaviour of Hostun sand. J Geotech Geoenviron Eng 2017;143(5):04017004. ASCE.
[37] Hardin BO, Drnevich VP. Shear modulus and damping in soils: design equation and curves. J. Soil Mech. Found. Eng. Div. 1972;98(SM7):667–92. ASCE.
[38] Viggiani GMB, Atkinson JH. Stiffness of fine-grained soil at very small strains. Geotechnique 1995;45(2):249–65.
[39] Skempton AW. Discussion of the planning and design of the new Hong Kong airport. Proc Inst Civ Eng 1957;7:305–7.
[40] Madabhushi SPG, Houghton NE, Haigh SK, Gould E. Development of a servo-hydraulic earthquake actuator for the Cambridge turner beam centrifuge. Int J Phys Model Geotech 2012;12(2):77–88.
[41] Gaudio D, Rampello S. Equivalent seismic coefficients for caisson foundations supporting bridge piers. Soil Dynam Earthq Eng 2020;129:105955. https://doi.org/10.1016/j.soildyn.2019.105955.
[42] Veletsos AS, Meek JW. Dynamic behavior of building-foundation systems. Earthq Eng Struct Dynam 1974;3(2):121–38.
[43] Idriss IM, Seed HB. Response of horizontal soil layers during earthquakes. J. Soil Mech. Found. Div., ASCE 1968;94(SM4):1003–31.
[44] Callisto L. MARTA v. 1.1: a computer program for the site response analysis of a layered deposit. 2015. https://drive.google.com/file/d/11pERKW4ZXkfOZmGhrYOWC_E7ocdjenDS/view.
[45] Darendeli GMB. Development of a new family of normalized modulus reduction and material damping curves. PhD dissertation. University of Texas at Austin; 2001.

[46] Gerolymos N, Gazetas G. Winkler model for lateral response of rigid caisson foundations in linear soil. Soil Dynam Earthq Eng 2006;26(5):347–61.
[47] Conti R, Di Laora R. Substructure method revisited for analyzing the dynamic interaction of structures with embedded massive foundations. J Geotech Geoenviron Eng 2022;148(6):04022029. ASCE.
[48] Gaudio D, Rampello S. On the assessment of seismic performance of bridge piers on caisson foundations subjected to strong ground motions. Earthq Eng Struct Dynam 2021;50(5):1429–50. https://onlinelibrary.wiley.com/doi/full/10.1002/eqe.3407.
[49] Stockwell RG, Mansinha L, Lowe RP. Localization of the complex spectrum: the S transform. IEEE Trans Signal Process 1996;44(4):998–1001.